Electrical linewidth metrology for systematic CD variation characterization and causal analysis

Jason P. Cain and Costas J. Spanos

Department of Electrical Engineering and Computer Sciences
University of California, Berkeley, CA 94720

ABSTRACT

Control of critical dimension (CD) variation is of extreme importance in modern semiconductor manufacturing processes. To be controlled, the nature of CD variation must be understood. This paper outlines a method for characterizing systematic spatial variation by means of dense electrical linewidth measurements, including actual sample data. In addition, since exhaustive sampling is prohibitively expensive for routine use, a method is discussed for finding an optimum economical sampling plan and using this plan to track systematic CD variation over time.

Keywords: Electrical linewidth metrology, critical dimension variation, CD variation, optimum sampling plan, photolithography

1. INTRODUCTION

As feature sizes continue to decrease in modern lithography processes, the ability to maintain control over the variation of critical dimensions (CD) becomes increasingly important. According to the 2002 update to the ITRS Roadmap [1], gate CD must be controlled to 3.7 nm (3σ) for the 100 nm node expected in 2003, a level for which no manufacturable solution is available. In order to control CD variation, the variation must first be characterized to determine its spatial and temporal nature. CD variation also has systematic and random components. The systematic components are of special interest, since they reveal critical process limitations relating to optics, mask making, bake control, etc. Because of that, it is desirable to track changes in the systematic variation components over time.

This paper outlines a framework for characterizing systematic variation in a gate patterning process, focusing primarily on systematic spatial variation using electrical linewidth metrology. Although similar work has been done previously [2,3], our work includes a novel modeling approach for components of systematic variation. A systematic variation model is described in section 2, followed by the experimental design needed to validate it in section 3. The experimental results are briefly described in section 4, followed by a method for finding an optimal economical sampling plan in section 5. Finally, conclusions will be presented in section 6.

2. SYSTEMATIC VARIATION MODEL

A variety of sources throughout the semiconductor manufacturing process contribute to overall CD variation, including mask errors [4,5], lens aberrations [6,7], scanner illumination variations [8,9], PEB temperature non-uniformity [10], and plasma etch rate non-uniformity, to name only a few. While some of the variation is assumed to be random, it has become apparent that much of the variation in the lithographic patterning process is systematic (*i.e.*, not due to chance, and thus repeatable) in nature. This gives hope that if the sources of the systematic variation can be found, methods for controlling systematic variation can be developed.

Systematic CD variation has been found at several different scales in the lithographic patterning process. One type of systematic variation that has received much attention is variation within the lithographic field. This type of variation affects each field on the wafer in the same way, and may be related to the optics of the exposure system or to the mask used in the exposure. In addition, there may be systematic variation across the wafer as a whole. This type of variation may be due to non-uniformities in temperature during a processing step, film thickness non-uniformity, and other problems that affect the whole wafer. Systematic variation is also seen from wafer to wafer within a lot, possibly due to some tool problem that affects every

wafer processed on that tool. Finally, systematic variation can be seen over longer periods of time from lot to lot. This may be due to long-term machine drifts, operator practices, and similar long-term effects.
In order to help understand the nested character of the CD variation, the following model is proposed, in which the variation from the nominal CD at a given point on the wafer is assumed to be the sum of the nominal CD, plus each of the systematic variance components and a random component:

$$CD_{ijkl} = CD_{nom} + f_i + w_j + l_k + L_l + \varepsilon \tag{1}$$

where

$$i = 1 \ldots N_f, \quad j = 1 \ldots N_w, \quad k = 1 \ldots N_l, \quad j = 1 \ldots N_L, \text{ and } \quad \varepsilon \sim N(0, \sigma_\varepsilon^2).$$

The symbols used in this model are explained in Table 1~~Table 1~~. Note that the random variation ε is assumed to be normally distributed with mean 0 and variance σ_ε^2. In this paper, we focus on the spatial components of systematic variation (f_i and w_j in Eq. 1).

Table 1. List of symbols for systematic variation model given in Eq. 1.

Symbol	Meaning
CD_{ijkl}	CD at a given point on the wafer
CD_{nom}	True mean of all critical dimensions in the process
f_i	Across-field systematic variation at index *i* within the field
w_j	Across-wafer systematic variation at index *j* within the wafer
l_k	Systematic variation from wafer to wafer within a lot at index *k* within the lot
L_l	Systematic variation from lot to lot at index *l* within the manufacturing run
ε	Random variation (including variation in the measurement process)
N_f	Number of points sampled in the field
N_w	Number of fields sampled on the wafer
N_l	Number of wafers sampled in the lot
N_L	Number of lots sampled in the manufacturing run

3. EXPERIMENTAL DESIGN

An experiment was designed to evaluate systematic variation in the lithographic pattern transfer process. A mask was designed to allow for dense CD measurements with a variety of metrology methods. This mask was then used to print a number of wafers, which were then measured to extract systematic variation.
In order to characterize the systematic variation in the pattern transfer process, dense measurements are needed to obtain a detailed picture of CD variation (a "variance map") for each of the desired variance scales (across chip, across wafer, etc.). In addition, it is desirable to compare various metrology methods to evaluate their effectiveness in characterizing systematic variation.
With this in mind, a test mask was designed to facilitate the investigation of systematic linewidth variation through a 2^3 factorial experiment with pattern density (isolated and dense), orientation (horizontal and vertical), and the presence or absence of optical proximity corrections (OPC) as the three factors. This mask is composed of a group of test structures, or module, repeated many times. Each module consists of two similar sub-modules. Both sub-modules have eight test structures (two of each combination of pattern density and orientation) for measuring the linewidth either electrically or via CD-SEM. In addition, both sub-modules have a Van der Pauw structure for measuring the resistivity of the film in which the test structures are fabricated (polysilicon in the case of this experiment) to facilitate electrical linewidth metrology (ELM) [11]. The sub-modules also contain a variety of periodic gratings for scatterometry measurements and several lines that run the full width of the sub-module and are continuous across the mask, so that the wafer may be cross-sectioned at any point and still yield usable cross-sectional SEM

features. The factorial design is completed by alternating sub-modules (which are otherwise identical) between the presence or absence of OPC. A block diagram of the figure is shown in Figure 1~~Figure 1~~.
This module is then repeated in a 22×19 array across the mask. This array is designed to be large enough to cover the maximum field size for modern steppers and scanners. When the mask pattern is reproduced many times on the wafer using a stepper or scanner exposure system, the result is that many thousand linewidth test structures are created on the wafer. This allows a highly detailed linewidth variance map to be created.

4. EXPERIMENTAL RESULTS

A number of eight-wafer sub-lots were exposed over a period of a few weeks. The exposures were performed using a 248 nm lithography tool and had a resist target CD of 180 nm and a post-trim target CD of 130 nm. After development, the wafers were randomized into new lots of 24 wafers to eliminate the effects of temporal variation in the lithography process from subsequent processing steps. These wafers were measured using CD-SEM and scatterometry after development, after resist trim etch, and after poly etch. In addition, the wafers were measured after poly etch using electrical linewidth metrology (ELM), which offers increased speed over CD-SEM. ELM has previously been used to characterize systematic spatial variation, however, this work offers more complete metrology at each processing step along with complete wafer-processing history. The use of multiple metrology methods allows for a comparison of the effectiveness of each method, as well as investigation of the correlation between methods. Also, care was taken to record the processing history of each wafer in detail in order to allow find similarities in processing which might account for a systematic variation signature. Results from one of these 24-wafer lots (a baseline trim etch lot) are presented in this study.
After the completion of wafer processing and CD-SEM and scatterometry measurements, the wafers were measured using ELM with an "exhaustive" sampling plan. The exhaustive sampling plan is designed to allow a very high degree of spatial resolution to provide detailed variance maps. This plan measures DUT1 (horizontal isolated), DUT3 (vertical isolated), and DUT4 (vertical dense) features for the no-OPC sub-modules. These features were chosen to match the features measured on the mask. The OPC sub-modules were not sampled due to the fact that some OPC features (particularly dense features) did not print correctly.
Every module in the field (22 rows × 14 columns = 308 modules per field as printed) was measured, and every field on the wafer (23 fields) was sampled. This means that the total number of measurements in the exhaustive sampling plan is 3 features/module × 308 modules/field × 23 fields/wafer = 21,252 features/wafer. The measurements are performed on an Electroglas autoprobe with an Agilent 4142B source/monitor unit. The required measurement time for this sampling plan is about 24 hours and 45 minutes per wafer. The first five wafers from the lot were measured using this plan.
The first step in characterizing the systematic variation is to calculate the "average" wafer (Figure 2~~Figure 2~~). This is calculated by averaging the ELM measurements for the five exhaustively sampled wafers at each point on the wafer. Inspection of the CD contour maps for the five wafers showed that the wafers were similar enough to justify averaging them together. The average wafer contour map in Figure 2~~Figure 2~~ reveals that there is a spot effect in the center of the wafer where the CD is smaller than the surrounding fields. Also, the right edge shows a smaller CD than the rest of the wafer. Note that the CD values in Figure 2~~Figure 2~~ are much smaller than the target CD of 130 nm due to the bias between electrical and physical CD [12].
The next step is to use this information to calculate the "average"' field by averaging the CD measurements for the five wafers at each point in the field (Figure 3~~Figure 3~~). Fields that seem atypical (those in the center and at the far right edge) are excluded in calculating the average field.
At this point measurements of the ELM2 mask can be used to isolate the effects of mask errors. As previous works have shown, the mask errors are magnified by the mask error factor (MEF) [13]. However, the MEF applies to the aerial image, whereas electrical measurements are performed after several subsequent processing steps. Therefore, the aerial image MEF may not be the correct factor to use in scaling the mask errors.
For the purposes of this analysis, we are defining the mask error *scaling* factor (MESF), which is the factor which minimizes the variance of the residuals when the scaled mask errors are subtracted from the average field data. Figure 4~~Figure 4~~ shows the variance of the residuals for varying scaling factors. The value of the scaling factor that minimizes the variance of the residuals is found to be 0.68. The mask errors scaled

by the appropriate factor are shown in Figure 5~~Figure 5~~. The scaled mask errors are then subtracted from the average field data (Figure 6~~Figure 6~~). The remaining variance is assumed to be the result of other imperfections in the imaging system (e.g. lens aberrations, illumination variations, etc.).
An ANOVA model is used in an attempt to extract the across-field systematic variation. The model chosen for the treatment effect is of the form

$$f(x_f, y_f) = a \cdot x_f^2 + b \cdot y_f^2 + c \cdot x_f + d \cdot y_f \tag{2}$$

where (x_f, y_f) are coordinates within the field in millimeters and a, b, c, and d are coefficients to be estimated using linear regression. The parameter estimates from the model fit are shown in Table 2~~Table 2~~, while an ANOVA table for the fit is shown in Table 3~~Table 3~~. In addition, a graphical representation of this model is shown in Figure 7~~Figure 7~~.

Table 2. Linear regression parameter estimates for across-field polynomial model shown in Eq. 2.

Parameter	Estimate	Standard Error	*p*-value
Intercept	55.58 nm	0.0515	< 0.0001
x_f^2	0.0019 nm/mm^2	0.0004	< 0.0001
y_f^2	0.0264 nm/mm^2	0.0006	< 0.0001
x_f	-0.0408 nm/mm	0.0122	0.0008
y_f	-0.6225 nm/mm	0.0154	< 0.0001

Table 3. ANOVA table for across-field polynomial model.

Source	DOF	Sum of Squares	Mean Square	F Ratio
Model	5	0.521×10^5	10420	369.15
Error	34414	9.714×10^5	28.227	***p*>F**
Total	34419	1.0235×10^6		<0.0001

This across-field systematic variation model is then subtracted from the average field data with scaled mask errors removed. The results are shown in Figure 8~~Figure 8~~.
The scaled mask errors and the polynomial model of across-field systematic variation can then be subtracted from each field in the average wafer data shown in Figure 2~~Figure 2~~. The results are shown in Figure 9~~Figure 9~~.
The wafer map in Figure 9~~Figure 9~~ reveals a localized effect in the center of the wafer where the CD is smaller than the surrounding area. An ANOVA model is again used to model this effect. A bivariate Gaussian is used to model the treatment effect. This model is of the form

$$CD(x_w, y_w) = \frac{c_1}{2\pi\sigma_x\sigma_y\sqrt{1-\rho^2}} \exp\left[-\frac{z}{2(1-\rho)^2}\right] + c_2\,, \tag{3}$$

$$\rho = \frac{\sigma_{xy}}{\sigma_x\sigma_y}\,, \tag{4}$$

$$z = \frac{(x_w - x_c)^2}{\sigma_x^2} - \frac{2\rho(x_w - x_c)(y_w - y_c)}{\sigma_x\sigma_y} + \frac{(y_w - y_c)^2}{\sigma_y^2}\,, \tag{5}$$

where (x_w, y_w) are coordinates on the wafer surface with origin at the center of the wafer, c_1 is a scaling factor, c_2 is a constant term, (x_c, y_c) is the center of the Gaussian function, σ_x and σ_y describe the "spread" of the Gaussian in the x and y directions, respectively, and σ_{xy} is an interaction term between spread in the x and y directions. This model is fit to the data using nonlinear regression. The parameter estimates from the model fit are shown in Table 4~~Table 4~~, and an ANOVA table is shown in Table 5~~Table 5~~. In addition, a graphical representation of the model is shown in Figure 10~~Figure 10~~. The bivariate Gaussian model is then subtracted from the average wafer with across-field effects removed, and the results are shown in Figure 11~~Figure 11~~.

Table 4. Nonlinear regression parameter estimates for bivariate Gaussian model shown in Eq. 3-5.

Parameter	Estimate
c_1	-1391.04
c_2	54.51 nm
x_c	1.71 nm
y_c	6.26 nm
σ_x	5.13 nm
σ_y	8.17 nm
σ_{xy}	27.12 nm^2

Table 5. ANOVA table for center spot Gaussian model shown in Eq. 3-5.

Source	DOF	Sum of Squares	Mean Square	F Ratio
Model	7	9.2×10^3	1314.29	47.06
Error	34414	9.611×10^5	27.93	***p*>F**
Total	34408	9.714×10^5		<0.0001

Finally, another ANOVA model is used to extract the remaining across-wafer systematic variation. A second-order polynomial model was chosen to model this treatment, and it is of the form:

$$w(x_w, y_w) = a \cdot x_w^2 + b \cdot y_w^2 + c \cdot x_w + d \cdot y_w + e \cdot x_w \cdot y_w \quad , \tag{6}$$

where (x_w, y_w) are coordinates on the wafer in millimeters and a, b, c, d, and e are coefficients to be estimated using linear regression. The parameter estimates from the model fit are shown in Table 6~~Table 6~~, and an ANOVA table for the fit is shown in Table 7~~Table 7~~. A graphical representation is shown in Figure 12~~Figure 12~~.

Table 6. Linear regression parameter estimates for across-wafer polynomial model shown in Eq. 6.

Parameter	Estimate	Standard Error	*p*-value
Intercept	55.59 nm	0.0515	< 0.0001
x_w^2	-0.00055 nm/mm^2	0.00002	< 0.0001
y_w^2	-0.00021 nm/mm^2	0.00002	< 0.0001
x_w	-0.0281 nm/mm	0.0007	< 0.0001
y_w	0.0137 nm/mm	0.0007	< 0.0001
$x_w y_w$	-0.00009 nm/mm^2	0.00003	0.0002

Table 7. ANOVA table for across-wafer polynomial model.

Source	DOF	Sum of Squares	Mean Square	F Ratio
Model	6	6.72×10^4	11200	430.99
Error	34402	8.94×10^5	25.99	***p*>F**
Total	34408	9.61×10^5		<0.0001

This across-wafer polynomial model is subsequently removed from the data, and the results are shown in Figure 13~~Figure 13~~. The remaining variance is assumed to be random. A summary ANOVA table of the systematic variation extracted from the lot is shown in Table 8~~Table 8~~, while a Pareto chart showing the components of CD variation present in the lot is shown in Figure 14~~Figure 14~~.

Table 8. Summary ANOVA table for systematic variation.

Source	DOF	Sum of Squares	Mean Square	F Ratio	*p*-value
Mask Errors	305	2.36×10^5	773.77	29.77	< 0.0001
Field Polynomial	5	5.21×10^4	10420	400.92	< 0.0001
Wafer Gaussian	7	9.20×10^3	1314.29	50.57	< 0.0001
Wafer Polynomial	6	6.72×10^4	11200	430.93	< 0.0001
Error	34401	8.94×10^5	25.99		

5. OPTIMUM ECONOMICAL SAMPLING PLAN SELECTION

It is not generally practical to measure all of the test structures on the ELM2 test wafers. For example, consider the cost of exhaustively measuring an entire wafer patterned with the ELM2 mask. Each module contains 16 features, and there are 22×14 = 308 modules per field (N_f = 308 in Equation 1). If the each wafer has 23 complete fields (N_w = 23), this corresponds to 113,344 features per wafer. This would take several days to measure even with high-speed electrical measurements, and possibly an order of magnitude longer using CD-SEM. In a high-volume production environment processing tens of thousands of wafers per month, this would be out of the question. Even the "exhaustive" sampling plan used to characterize systematic variation required over 20,000 measurements (roughly 25 hours of measurement time). Clearly, this is not a practical solution.

Therefore, decisions must be made concerning how many structures to measure and how to distribute the measurements across the wafer. The need to accurately capture the systematic variance must be balanced against the cost of making the measurements. Knowledge about the structure of the systematic variance allows the selection of a so-called optimum sampling plan that will "best" capture the systematic variance at a fixed cost.

Once a detailed variance map has been created and the systematic variance has been extracted as described in section 3, an optimum sampling plan can be selected. The first step is to set a fixed measurement cost, *i.e.* the maximum allowable measurement time for each wafer. This is important because it describes the delay in processing required to measure each wafer, and increased delay means that the wafer throughput (and, therefore, profit) is decreased. In setting the measurement cost, the need to sample each wafer many times (requiring a high measurement cost per wafer) to capture within-wafer systematic variation must be balanced against the need to sample many wafers (requiring a low measurement cost per wafer) to capture wafer-to-wafer systematic variation.

Once a fixed cost is determined, different sampling plans that have the same cost but varying distributions of the measurements can be evaluated. This is done by trying the sampling plans on the data from the exhaustively sampled wafers and fitting the various systematic variation models to the data from the reduced sampling plans. The best plan is then defined as the plan that obtains the best fit for the different models. One measure of best fit is the length of the 95% confidence intervals for the different model parameters. Of course, different priority may be given to different model parameters, and this may be taken into account when selecting the best plan.

To test this method, four "economical" sampling plans were designed. These plans are summarized in Table 9~~Table 9~~ and shown graphically in Figure 15~~Figure 15~~. Note that these sampling plans have roughly the same number of measurements and take about one hour to measure (recall that the exhaustive plan required nearly 25 hours).

Table 9. Summary of economical sampling plans.

	Points per Field	Fields per Wafer	Total Measurements

Plan 1	40	23	920
Plan 2	60	15	900
Plan 3	103	9	927
Plan 4	154	5	785

These plans were used to analyze the respective subset of the complete data set generated by the exhaustive sampling plan. The polynomial models for across-field and across-wafer systematic variation were fitted to the sampled data sets, and the widths of the 95% confidence intervals were compared. The results are shown in Figure 16~~Figure 16~~. Only Plan 1 was able to successfully estimate all of the parameters of the across-wafer systematic variation, and still obtains a good estimate of the across-field parameters compared to the other economical plans. Therefore, this is the most appropriate plan to use if the goal is to characterize both across-field and across-wafer systematic variation. Although this simple example serves to illustrate the concept of finding an "optimum" sampling plan, a more complete implementation would include an optimizing algorithm to compare many more sampling plans to find a better optimum.

6. CONCLUSIONS

Electrical linewidth metrology with an exhaustive sampling plan was used to characterize spatial CD variation in a lithographic patterning process. Mask errors were the largest source of systematic variation present in the process, although the mask errors seem to be de emphasized on the final product because of the interaction between the aerial image and the final poly features. There are also significant systematic across-field and across-wafer components of spatial variation which may be modeled with simple basis functions such as polynomials. A wafer center-spot effect, most likely an artifact of the developing fluid dispense mechanism, was also modeled using a bivariate Gaussian.

The information gained in the systematic variation characterization was then used to select a reduced economical sampling plan. This plan may then be used to track changes in the systematic variation present in the process.

ACKNOWLEDGEMENTS

This work was performed in partnership with the National Institute for Standards and Technology (98-01-0167). The authors would like to thank Matt Hankinson, Joe Bendik, and Will Conley for their help in preparing this work. The electrical linewidth measurements were performed in the Device Characterization Laboratory, a part of the UC Berkeley Microfabrication Laboratory.

REFERENCES

1. International Technology Roadmap for Semiconductors. http://public.itrs.net
2. C. Yu, T. Maung, C. J. Spanos, D. S. Boning, J. E. Chung, H.-y. Liu, and K.-J. Chang, "Use of short-loop electrical measurements for yield improvement," *IEEE Trans. Semiconduct. Manufact.* **8**, pp. 150-159, May 1995.
3. A. K. Wong, A. F. Molless, T. A. Brunner, E. Coker, R. H. Fair, G. L. Mack, S. M. Mansfield, "Linewidth variation characterization by spatial decomposition," *J. Microlith., Microfab., Microsyst.*, **1**(2), pp. 106-116, July 2002.
4. A. K. Wong, R. A. Ferguson, L. W. Liebmann, S. M. Mansfield, A. F. Molless, M. O. Neisser, "Lithographic effects of mask critical dimension error," in *Optical Microlithography XI*, ed. L. van den Hove, Proc. SPIE Vol. 3334, pp. 106-116 (1998).
5. F. M. Schellenberg, V. Boksha, N. Cobb, J. C. Lai, C. H. Chen, C. Mack, "Impact of mask errors on full chip error budgets," in *Optical Microlithography XII*, ed. L. van den Hove, Proc. SPIE Vol. 3679, pp. 261-275 (1999).
6. T. A. Brunner, "Impact of lens aberrations on optical lithography," *IBM J. Res. Develop.*, **41**(1/2), pp. 57-67, Jan./Mar. 1997.
7. B. W. Smith and R. Schlief, "Understanding lens aberrations and influences to lithographic imaging," in *Optical Microlithography XIII*, ed. C. Progler, Proc. SPIE Vol. 4000, pp. 294-306 (2000).

8. Y. Borodovsky, "Impact of local partial coherence variations on exposure tool performance," in *Optical/Laser Microlithography VIII*, T. A. Brunner, ed., *Proc. SPIE* **2440**, pp. 750-770, 1995.
9. T. C. Barrett, "Impact of illumination pupil-fill spatial variation on simulated imaging performance," in *Optical Microlithography XIII*, ed. C. Progler, Proc. SPIE Vol. 4000, pp. 804-817 (2000).
10. D. Steele, A. Coniglio, C. Tang, B. Singh, S. Nip, C. Spanos, "Characterizing post exposure bake processing for transient and steady state conditions, in the context of critical dimension control," in *Metrology, Inspection, and Process Control for Microlithography XVI*, ed. D. J. C. Herr, Proc. SPIE Vol 4689, pp. 517-530 (2002).
11. M. W. Cresswell, R. A. Allen, "Electrical CD metrology and related reference materials," in *Handbook of Silicon Semiconductor Metrology*, A. C. Diebold, ed., pp. 377-410, Marcel Dekker, Inc. (2001).
12. A. Grenville, B. Coombs, J. Hutchinson, K. Kuhn, D. Miller, P. Troccolo, "Electrical critical dimension metrology for 100-nm linewidths and below," in *Optical Microlithography XIII*, ed. C. Progler, Proc. SPIE Vol. 4000, pp. 452-459 (2000).
13. A. K. Wong, R. A. Ferguson, S. M. Mansfield, "The mask error factor in optical lithography," *IEEE Trans. Semiconduct. Manufact.* **13**, pp. 235-242, 2000.

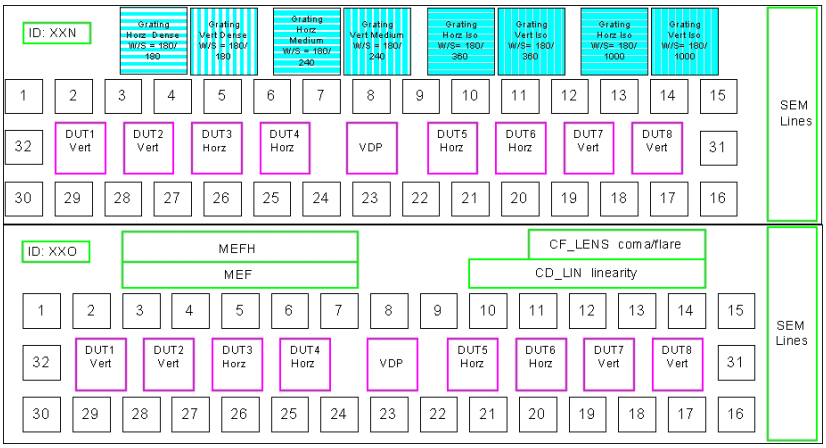

Figure 1. **Test mask module. The lower sub-module has OPC, while the upper sub-module does not.**

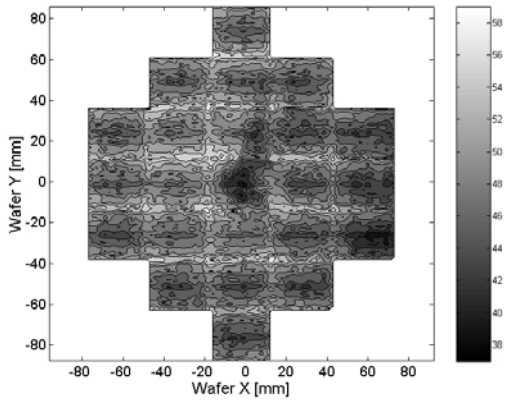

Figure 2. A CD contour map of the "average" wafer from the baseline trim etch lot. The average is computed by averaging the ELM measurements for the five exhaustively sampled wafers at each point on the wafer.

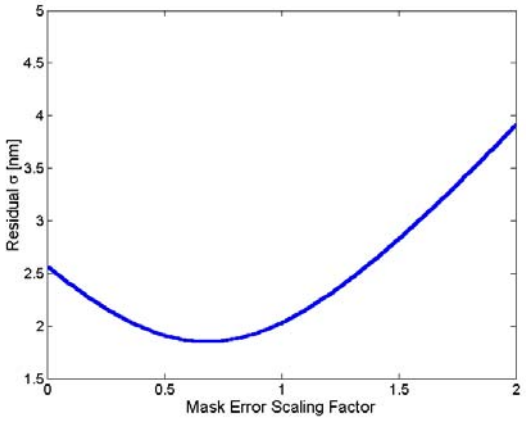

Figure 4. Plot used to find the mask error scaling factor which minimizes the variance of the residuals when the scaled mask errors are subtracted from the average field data.

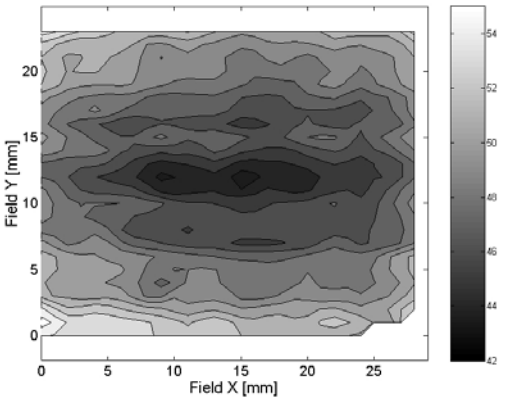

Figure 3. A CD contour map of the "average" field from the baseline trim etch lot. The average is computed by averaging the ELM measurements for the five exhaustively sampled wafers at each point in the field. Atypical fields are excluded in calculating the average.

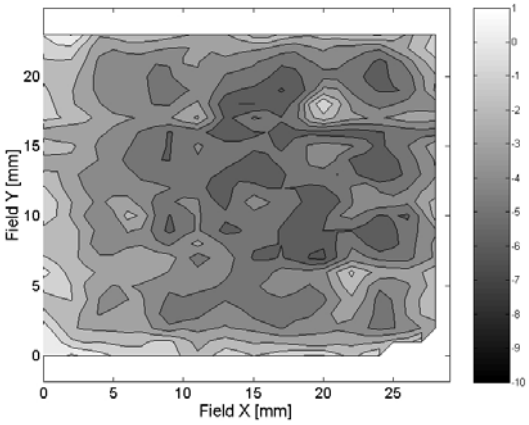

Figure 5. DUT3 (vertical isolated) feature mask errors scaled by the factor which minimizes variance in the residuals when the scaled mask errors are subtracted from the average field.

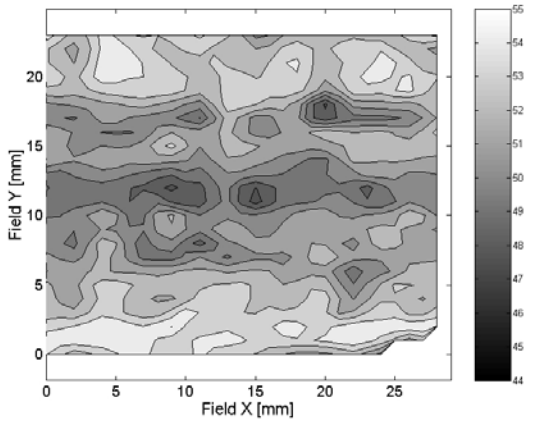

Figure 6. Average field with scaled mask errors removed.

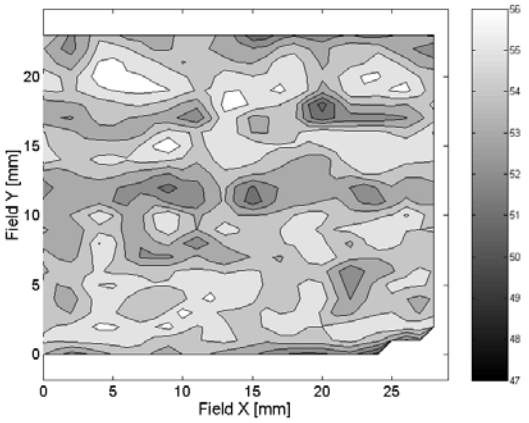

Figure 8. Residuals after the second-order polynomial model (Eq. 2) of across-field systematic variation is removed from average field data with scaled mask errors removed.

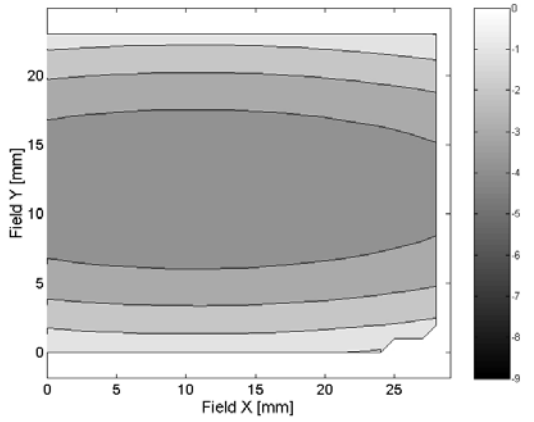

Figure 7. Graphical representation of second-order polynomial model (Equation 2) of across-field systematic variation for DUT3 (vertical isolated) features.

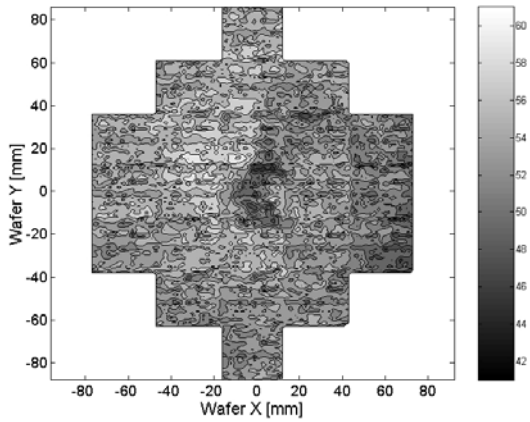

Figure 9. Average wafer after removal of scaled mask errors and polynomial model of across-field systematic variation from each field on the wafer.

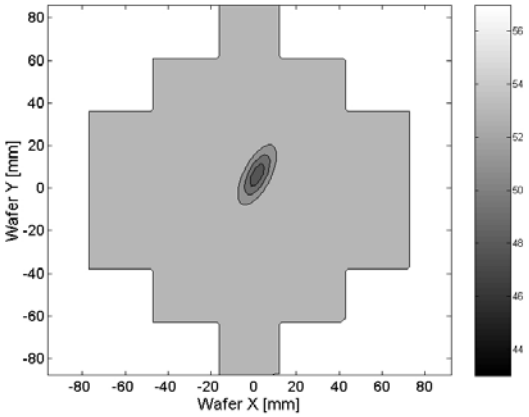

Figure 10. Graphical representation of bivariate Gaussian model used to model spot effect in the center of the wafer.

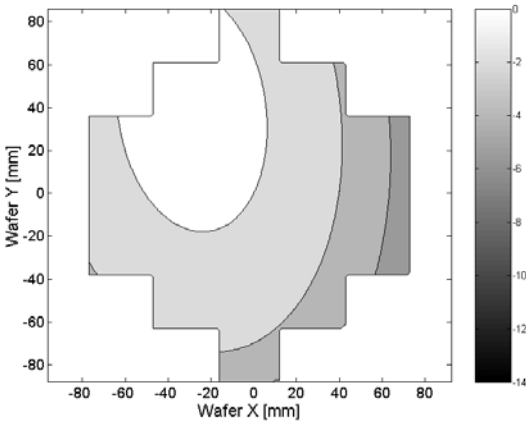

Figure 12. Graphical representation of second-order polynomial model (Eq. 6) of across-wafer systematic variation for DUT3 (vertical isolated) features.

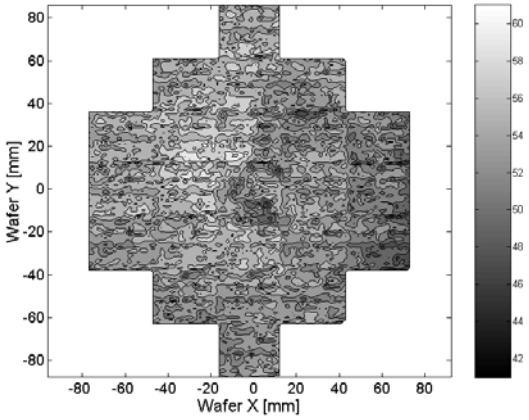

Figure 11. Average wafer after removal of across-field systematic variation and bivariate Gaussian spot effect model.

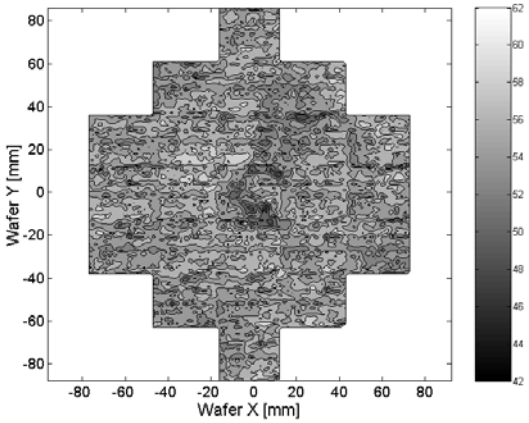

Figure 13. Residuals after removal of scaled mask errors, polynomial across-field systematic variation model, and Gaussian and polynomial across-wafer systematic variation models.

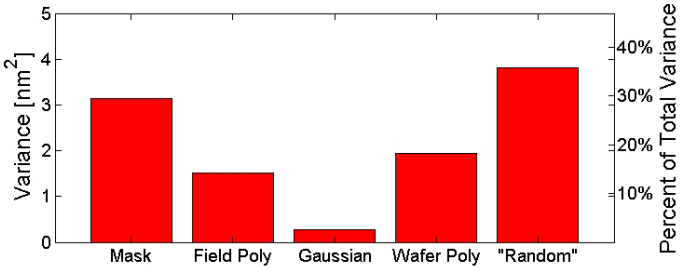

Figure 14. **Pareto chart of components of CD variation present in the process.**

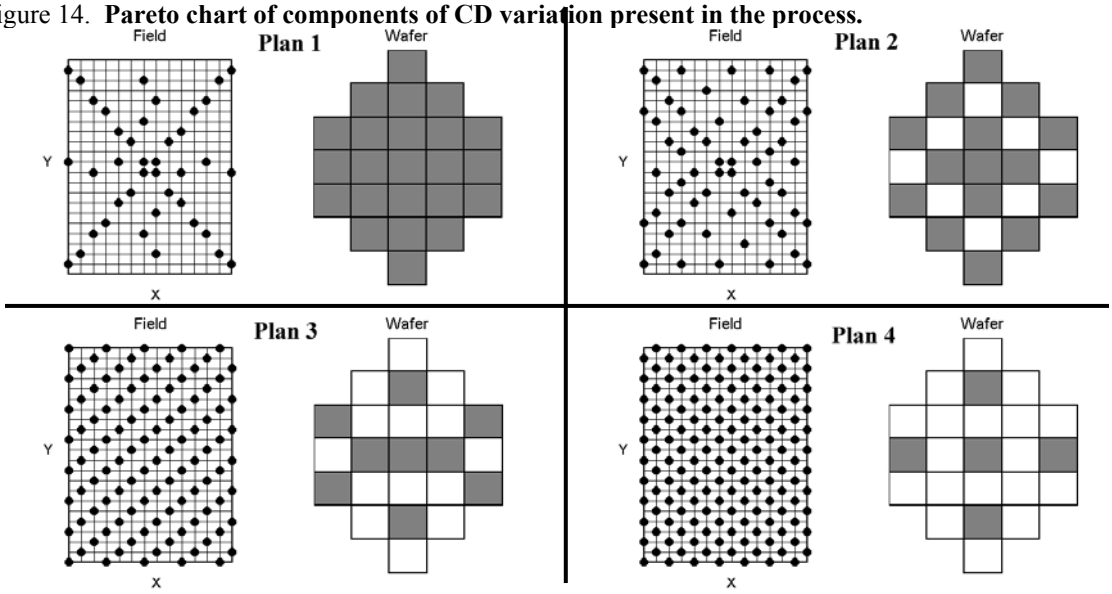

Figure 15. Candidate economical sampling plans.

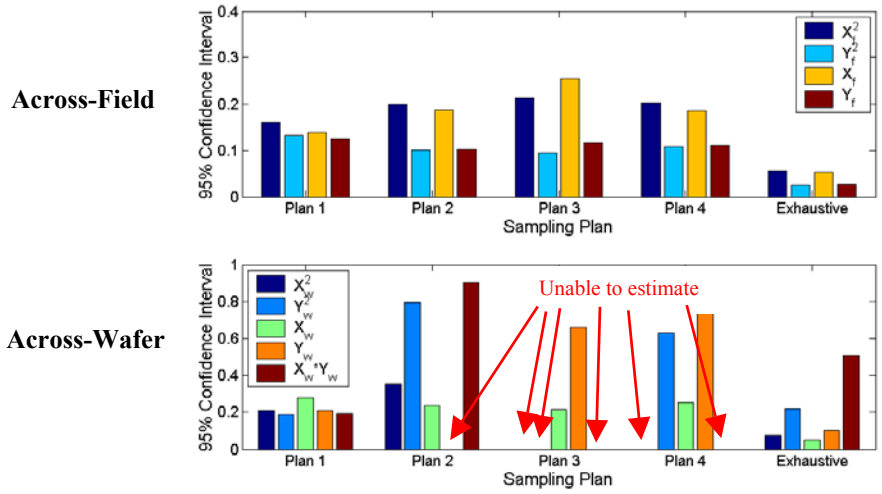

Figure 16. Comparison of candidate economical sampling plans. Vertical axis shows the relative width of the 95% confidence interval for each parameter estimate.